IEEE Access
Multidisciplinary | Rapid Review | Open Access Journal

Received March 4, 2021, accepted March 16, 2021, date of publication March 22, 2021, date of current version March 30, 2021.

Digital Object Identifier 10.1109/ACCESS.2021.3067649

Roll Stability and Path Tracking Control Strategy Considering Driver in the Loop

TONGLIANG XU[1] AND XUANYAO WANG[1,2]
[1]School of Mechanical Engineering, Anhui University of Science and Technology, Huainan 232001, China
[2]Shaanxi Automobile Holding Group Huainan Special Purpose Vehicle Co., Ltd., Huainan 232008, China

Corresponding author: Xuanyao Wang (xuanyaowang@126.com)

This work was supported in part by the Anhui Provincial Natural Science Foundation under Grant 1908085ME159, and in part by the Project funded by the Scientific Research Activities of Post-Doctoral Researchers in Anhui Province under Grant 2020B447.

ABSTRACT A study pointed out that the delay time of the driver's nervous system has a significant effect on the roll stability of the vehicle. However, the existing researches on vehicle rollover prevention control rarely consider the influence of driver factors on vehicle roll stability. Aiming at this problem, a vehicle roll stability and path tracking control strategy considering driver in the loop is proposed to assist different types of drivers. It includes the supervisory decision layer and execution layer. The supervisory decision layer selects the corresponding control mode according to the driver's steering wheel angle change rate, path tracking deviation and vehicle roll stability information. The execution layer includes three modes: human-machine shared steering, active braking and integrated chassis control. The human-machine shared steering and active braking modes assist the driver to improve the roll stability and path tracking accuracy. The integrated chassis control mode is used for the automatic driving of vehicles under emergency conditions. Simulation results show that the proposed control strategy can effectively improve the vehicle roll stability and path tracking accuracy, and reduce the driver's operating burden.

INDEX TERMS Roll stability, path tracking, human-machine sharing, coordinated control, integrated control.

I. INTRODUCTION

According to the statistics of the National Highway Traffic Safety Administration (NHTSA), there were 36560 people killed in motor vehicle traffic crashes on US roadways during 2018, and the 2018 number of large-truck occupant fatalities is the highest since 1988 [1]. Passengers in a rollover accident are 10 times more likely to die than a non-rollover accident [2]. Vehicles such as trucks and sport utility vehicles (SUV) are more prone to rollover accidents due to the characteristics of high centroid position, large mass and narrow wheel base. Therefore, researchers pay more and more attention to the roll stability control of the vehicle.

A variety of control methods have been proposed to the field of roll stability control, such as differential braking control [2], [3], active steering control [4], [5], suspension control [6], integrated chassis control [7], [8]. It can be seen from the above literature, although the existing anti-rollover control methods can reduce the risk of rollover, they ignore the path tracking problem. Due to the conflict between roll stability and path tracking [9], and in a word, the better the control effect, the worse the desired path tracking effect. If the vehicle deviates from the original path, it may collide with railings on both sides of the road or other vehicles, and causing new accidents. Thus, it is necessary to consider path tracking performance while improving vehicle roll stability [10]. Qian *et al*. [11] designed an integrated chassis controller by considering both anti-rollover and path tracking performance. The proposed control strategy can guarantee that the vehicle tracks the desired path well and effectively reduces the risk of rollover. Li *et al*. [12] developed an active safety cooperative control system with adaptive cruise control (ACC), rear wheel steering control (RSC) and rollover brake control (RBC). The proposed integrated control strategy has good path tracking performance and roll stability. Tian *et al*. [13] exploited a hierarchical adaptive control framework to coordinate the contradiction between path tracking and roll stability through steering control.

However, most of the literature on vehicle rollover prevention and path tracking control do not consider the impact of

The associate editor coordinating the review of this manuscript and approving it for publication was Chao-Yang Chen.

driver's behavior on vehicle rollover dynamics, only regard the driver's input as a kind of interference. On the one hand, experienced drivers can make decisions to prevent rollover according to their perceived rollover tendency. On the other hand, the driver cannot correct the vehicle rollover in time due to the limitation of psychological and physiological limits. It is necessary to consider the driver's behavior characteristics in vehicle roll stability and path tracking control. Jin *et al*. [14] established a dynamic model of the driver's roll response and analyzed the influence of driver perception, decision and execution parameters on vehicle roll stability, and the research results showed that the driver's nervous system delay time had a significant impact on roll stability. Cao *et al*. [15] designed a rollover prevention collaborative control strategy considering the features of different driver's manners. The proposed strategy can provide diverse control effects for different drivers, and effectively prevent vehicle rollover as well as realize favorable path tracking performance. However, the driver's physical or psychological characteristics are not considered. Therefore, it is necessary to design a control system suitable for drivers with different neural response delays to enhance roll stability while tracking the desired path, thereby reducing the driver's operating burden.

In the current research stage, in order to reduce the operating burden of the driver, the shared control considering human-machine interaction seems to be an available solution [16]. Hoc *et al*. [17] developed a human-machine cooperation framework and applied it to the field of vehicle automation. Sentouh *et al*. [18] designed a human-machine shared controller of lane keeping based on Lyapunov method. Chen *et al*. [19] presented a human-machine shared control method based on hybrid system theory to coordinate the conflict between human and lane departure assistance system. Wang *et al*. [20] considered diverse driving styles and devised a shared steering control law using an exponential function to lighten the burden on the driver when turning. Wang *et al*. [21] introduced the architecture of human-machine shared control, driver modeling and interaction strategy under driver-vehicle shared schemes, and further discussed the challenges and opportunities in the future. Nevertheless, human-machine shared control is mostly used in relatively stable scenarios such as lane keeping and does not consider the roll motion of vehicle [22], and there is a lack of research on shared control under emergency scenarios.

To solve these problems, this paper aims to assist the stability needs of drivers with different physiological or psychological states and introduces the human-machine shared control into roll stability and path tracking control. A roll stability control strategy considering the driver in the loop is proposed, so as to reduce the risk of vehicle rollover and track the desired path at the same time.

The rest of this article is arranged as follows: section II introduces the system model. The human-machine shared control rules and roll stability control strategy are designed in section III. The simulation results of control strategy are conducted in section IV and conclusions as well as future work are finally given in section V.

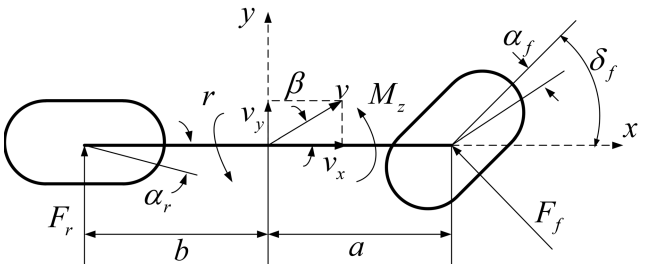

FIGURE 1. 2 DOF vehicle model.

II. SYSTEM MODEL

A. VEHICLE MODEL

As shown in Figure 1, the linear two degree-of-freedom (DOF) model is selected as the vehicle dynamics model, the state equation is given as follows:

$$\begin{bmatrix} \dot{\beta} \\ \dot{r} \end{bmatrix} = \begin{bmatrix} a_{11} & a_{12} \\ a_{21} & a_{22} \end{bmatrix} \begin{bmatrix} \beta \\ r \end{bmatrix} + \begin{bmatrix} \frac{2C_f}{mv_x} & 0 \\ \frac{2aC_f}{I_z} & \frac{1}{I_z} \end{bmatrix} \begin{bmatrix} \delta_f \\ M_z \end{bmatrix} \quad (1)$$

where

$$a_{11} = -\frac{2(C_f + C_r)}{mv_x}, \quad a_{12} = -1 - \frac{2(aC_f - bC_r)}{mv_x^2}$$
$$a_{21} = -\frac{2(aC_f - bC_r)}{I_z}, \quad a_{22} = -\frac{2(a^2C_f + b^2C_r)}{I_z v_x}$$

β is the centroid side slip angle; r is the yaw rate; C_f and C_r are the cornering stiffness constants of the front and rear tires, respectively; m is the total vehicle mass; v_x is the longitudinal speed; a and b are distances from the gravity center to the front and rear axles, respectively; I_z is the moment of inertia of yaw; δ_f is the front wheel steering angle; M_z is the yaw moment.

B. VEHICLE-ROAD MODEL

Assuming that vehicle is a rigid body, the longitudinal and lateral positions as well as the yaw angle of the vehicle are shown in Figure 2, more details can be seen in reference [23].

The speed of the vehicle's center of mass in the X axis and the Y axis direction of the ground coordinate system are as follows:

$$\begin{cases} \dot{X} = v_x \cos\psi - v_y \sin\psi \\ \dot{Y} = v_x \sin\psi + v_y \cos\psi \end{cases} \quad (2)$$

Assuming that vehicle yaw angle is small and tire force is in the linear region, so v_y is much smaller than v_x. It can be obtained equation (3) by replacing the X axis and the Y axis in the ground coordinate system with the x axis and the y axis in the vehicle coordinate system:

$$\begin{cases} \dot{x} = v_x \\ \dot{y} = v_x\psi + v_y \end{cases} \quad (3)$$

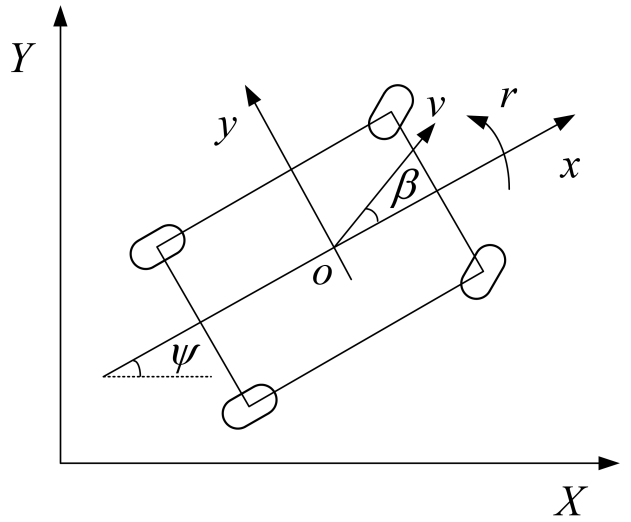

FIGURE 2. Vehicle kinematic relation.

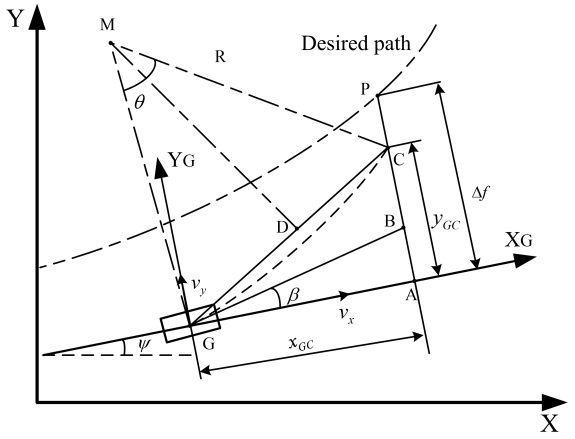

FIGURE 3. Vehicle trajectory prediction under the assumption of constant yaw rate.

$$\begin{cases} r = \dot{\psi} \\ \beta = \dfrac{v_y}{v_x} \end{cases} \tag{4}$$

where ψ is the yaw angle; v_y is the lateral velocity.

Combining equation (1) with equations (3)-(4), the state equation of vehicle-road model is obtained as follows:

$$\dot{x} = Ax + B\delta_f \tag{5}$$

where

$$x = \begin{bmatrix} v_y & r & y & \psi \end{bmatrix}^T$$

$$A = \begin{bmatrix} -\dfrac{2(C_f + C_r)}{mv_x} & -v_x - \dfrac{2(aC_f - bC_r)}{mv_x} & 0 & 0 \\ -\dfrac{2(aC_f - bC_r)}{I_z v_x} & -\dfrac{2(a^2C_f + b^2C_r)}{I_z v_x} & 0 & 0 \\ 0 & 0 & 0 & v_x \\ 0 & 1 & 0 & 0 \end{bmatrix}$$

$$B = \begin{bmatrix} \dfrac{2C_f}{m} & \dfrac{2aC_f}{I_z} & 0 & 0 \end{bmatrix}^T$$

C. DRIVER MODEL

It is very important to establish a reasonable and effective driver model for "driver-vehicle-road" closed-loop simulations. The driver model established in this paper assumes that the expected path is known, and a driver model based on trajectory prediction is established [24].

Assuming that the vehicle maintains a constant yaw rate for a period of time in the future, the vehicle will make a uniform circular motion. Figure 3 describes the predicted vehicle trajectory. Point G is the centroid position of the vehicle for the current time, point C is the centroid position of the vehicle after time t_p, and the trajectory between the two points is a circle of radius R. Point M is the center of the vehicle trajectory, θ is the center angle of the trajectory, P is the preview point on the desired path, and ψ is the heading angle of the vehicle for the current time. Δf is the lateral deviation at the vehicle preview point, GB is tangent to the vehicle trajectory at point G.

It can be seen from Figure 3 that $\angle CGA = \angle CGB + \beta$, $\angle CGB$ is the chord tangent angle of the vehicle's circle trajectory, we can get $\angle CGA = \theta/2 + \beta$, then

$$y_{GC} = \tan\left(\frac{\theta}{2} + \beta\right) x_{GC} \tag{6}$$

After time t_p, the ideal position of the vehicle centroid should be point P, that is $\angle PGA = \angle CGA$, $y_{GC} = \Delta f$. Since it is assumed that the vehicle moves in a uniform circular motion, by $\theta = rt_p$. And because $v_y \ll v_x$, by $x_{GC} \approx v_x t_p$. The expected steering wheel angle is:

$$\delta_{sw}^d = \frac{r_d}{G_r} = \frac{2\left[\arctan\left(\frac{\Delta f}{v_x t_p}\right) - \beta\right]}{t_p G_r} \tag{7}$$

where $G_r = \frac{v_x}{iL(1+Kv_x^2)}$; $K = \frac{m(bC_r - aC_f)}{2C_f C_r L^2}$; i is the steering ratio; $L = a + b$.

There is a deviation between the current yaw rate and the expected yaw rate $\Delta r = r_d - r$, and the driver applies an additional steering wheel angle $\Delta\delta_{sw}$ to compensate for yaw rate deviation, that is $\Delta r = K_r \Delta\delta_{sw}$.

The ideal steering wheel angle is:

$$\delta_{sw}^* = \delta_{sw}^d + \Delta\delta_{sw} \tag{8}$$

where K_r is the feedback coefficient, $K_r = G_r$.

The driver's physiological limitation mainly comes from the reaction lag and action response lag. Neural response lag is usually a pure lag, which can be represented by the transfer function $e^{(-t_d s)}$ and a physical limitation, which is a first-order lag $1/(1 + t_h s)$. The actual steering angle is defined as:

$$\delta_{sw} = \frac{e^{-t_d s}}{1 + t_h s}\delta_{sw}^* \tag{9}$$

where t_d is neural response lag time constant, t_h is action response lag time constant.

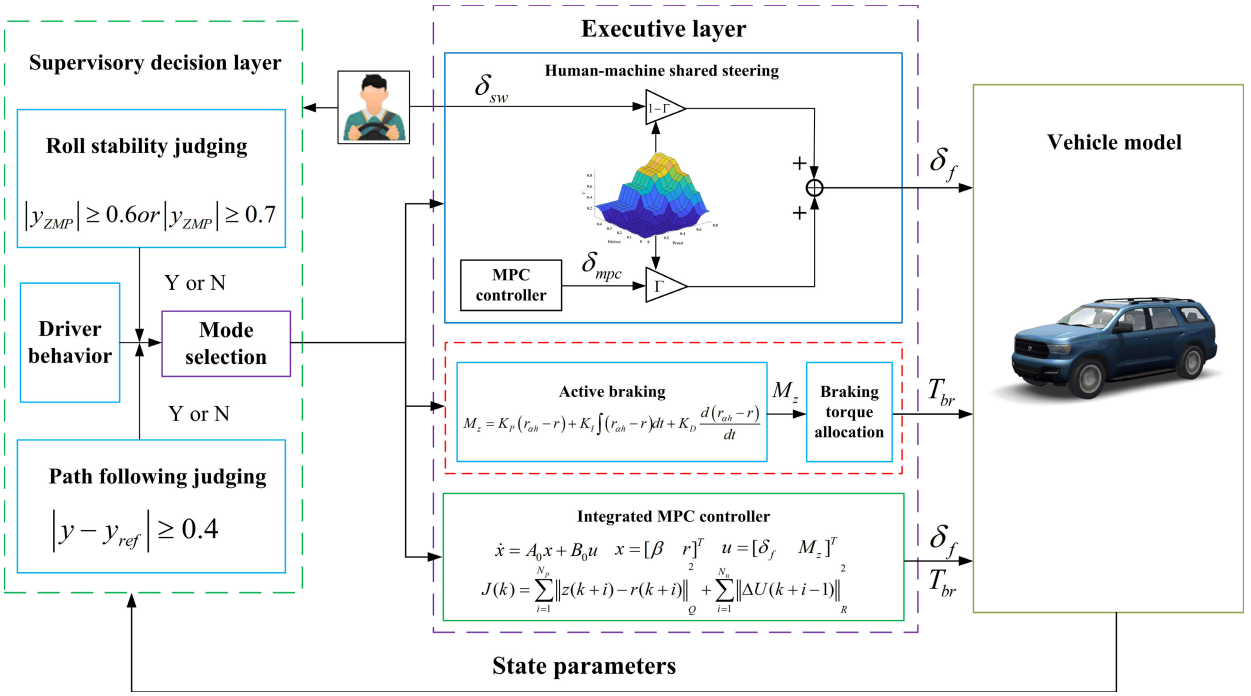

FIGURE 4. General architecture.

III. DESIGN OF CONTROL FRAMEWORK

According to the established system model and roll stability evaluation index, the roll stability and path tracking controllers adapted to different types of drivers are designed. The diagram of general architecture is shown in Figure 4. It is assumed that the vehicle studied in this work is equipped with a steer-by-wire and active braking system, and has an automatic driving function. Vehicle state parameters and road information (such as side slip angle, body roll angle, road curvature, roll angle acceleration) required for controller design can be measured, the specific structure of steering and brake system as well as the observation of state parameters are not involved in this work.

A. EVALUATION INDEX OF ROLL STABILITY

The supervisory decision layer is responsible for detecting steering wheel angle signal and vehicle status signal. Then, the input signal is compared with the set safety threshold and the corresponding control mode is selected.

The challenge of rollover prevention is that it is difficult to predict the moment when roll occurs, especially when there are time-varying road curvature and lateral slope angle. This section adopts the roll stability criterion based on zero moment point represented by literature [25].

As shown in Figure 5, the analysis of vehicle roll stability mainly focuses on the lateral offset of zero moment point.

The following equations can be obtained according to the roll moment balance relative to zero moment point.

$$mg\cos(\phi)\bar{y}_{ZMP} = [ma_y + mg\sin(\phi)]h - I_x\ddot{\phi} \quad (10)$$

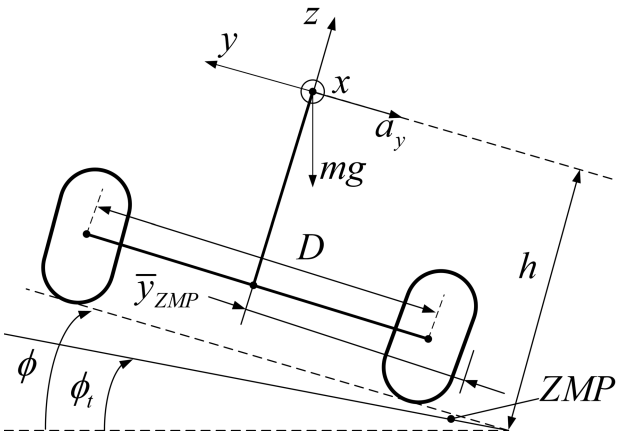

FIGURE 5. Rigid vehicle model on banked surface.

$$a_y = \dot{v}_y + rv_x \quad (11)$$

Considering that ϕ is small, it can be assumed that $\cos(\phi) \approx 1$ and $\sin(\phi) \approx \phi$, the following equation can be derived from equations (10) and (11):

$$\bar{y}_{ZMP} = h\phi + \frac{h}{g}(\dot{v}_y + rv_x) - \frac{I_x}{mg}\ddot{\phi} \quad (12)$$

The lateral offset of zero moment point is normalized to half of the track width:

$$y_{ZMP} = \frac{2}{D}[h\phi + \frac{h}{g}(\dot{v}_y + rv_x) - \frac{I_x}{mg}\ddot{\phi}] \quad (13)$$

where ϕ and ϕ_t are the roll angle of vehicle and road, respectively. a_y is lateral acceleration; I_x is the moment of inertia of

TABLE 1. Mode selection.

Selection conditions		Shared control	Active braking
$\int\lvert\dot{\delta}\rvert dt < Th$	$\lvert y-y_{ref}\rvert < 0.4m$ and $\lvert y_{ZMP}\rvert < 0.6$	Close	Close
	$\lvert y-y_{ref}\rvert \geq 0.4m$ and $\lvert y_{ZMP}\rvert < 0.6$	Open	Close
	$\lvert y-y_{ref}\rvert < 0.4m$ and $\lvert y_{ZMP}\rvert \geq 0.6$	Close	Open
	$\lvert y-y_{ref}\rvert \geq 0.4m$ and $\lvert y_{ZMP}\rvert \geq 0.6$	Open	Open
$\int\lvert\dot{\delta}\rvert dt \geq Th$ and $\lvert y_{ZMP}\rvert \geq 0.7$		Integrated chassis control	

vehicle body around the x axis; h is the height of centroid; D is the equivalent wheelbase of the vehicle. The range of y_{ZMP} is $[-1, 1]$, $y_{ZMP} = 0$ means the vehicle has no roll, $y_{ZMP} = \pm 1$ means one side of vehicle lift off road. Similar to the threshold values set in [26], the threshold value is set as 0.6 and 0.7.

The mode selection method proposed in this work is as follows: According to the change rate of the steering wheel angle over a period of time, the vehicle's roll stability and path tracking deviation, it is compared with the safety threshold. When the change rate of steering wheel angle over a period of time is less than Th, it is considered that the driver's physiological and psychological state is in the normal range and the driver has the ability to continue to manipulate the vehicle, where $Th = 500\,\mathrm{deg}/s$. If the difference between the actual lateral position and the ideal lateral position is greater than 0.4 m, it is considered that the vehicle deviates from the desired path, and the human-machine shared controller is turned on. Otherwise, the human-machine shared controller is turned off. If $|y_{ZMP}| \geq 0.6$, it is considered that roll stability is poor, and active braking controller is turned on to improve roll stability. Otherwise, active braking controller is turned off. When the change rate of steering wheel angle is greater than Th, it is considered that the driver is in a state of tension and panic, and the ability to continue driving the vehicle is poor. If $|y_{ZMP}| \geq 0.7$, the vehicle enters an autonomous driving state, and the safety system completely takes over the vehicle. Table 1 shows the switching strategy of the control mode in the supervisory decision layer.

B. DESIGN OF STEER-BY-WIRE CONTROLLER

A steer-by-wire controller is designed to track the desired path by adjusting the front wheel angle when the vehicle deviates from the desired path. Model predictive control (MPC) can calculate the dynamics state of the vehicle for the future, and it has preponderance in handling constrained control targets. Through rolling optimization strategy, it can recompense the non-determinacy caused by model destabilization and discrepancy, so as to acquire better dynamic control function and guarantee the vehicle's stability. Hence, MPC is utilized to design the steer-by-wire controller in this section.

1) MPC CONTROLLER DESIGN

The vehicle-road model in section II B is adopted as the predictive model of MPC. When the vehicle runs into the nonlinear region, the modeling inaccuracy will expand. However, the goal of steering control is to ensure that the vehicle runs in a linear region, which can be satisfied by the constraints of MPC optimization. Therefore, the assumptions in section II B are appropriate. Then, by discretizing (5) at the sample time T_s using a zero-order hold method; the discrete-time model can be obtained as follows:

$$x(k+1) = A_d x(k) + B_d \delta_f(k) \tag{14}$$

Defining lateral displacement and yaw angle as output, by:

$$z(k) = C_d x(k) \tag{15}$$

where $A_d = e^{AT_s}$; $B_d = \int_0^{T_s} e^{A\tau} d\tau \cdot B$ and C_d are the discrete matrices.

$$z(k) = \begin{bmatrix} y(k) \\ \psi(k) \end{bmatrix}; \quad C_d = \begin{bmatrix} 0 & 0 & 1 & 0 \\ 0 & 0 & 0 & 1 \end{bmatrix}$$

Assuming that the prediction predictive horizon is N_p, the control predictive horizon is N_u, and $N_u \leq N_p$. In this case, the future vehicle states could be predicted as follows:

$$\begin{cases} x(k+1) = A_d x(k) + B_d \delta_f(k) \\ x(k+2) = A_d^2 x(k) + A_d B_d \delta_f(k) + B_d \delta_f(k+1) \\ \quad \vdots \\ x(k+N_u) = A_d^{N_u} x(k) + A_d^{N_u-1} B_d \delta_f(k) \\ \quad + A_d^{N_u-2} B_d \delta_f(k+1) + \cdots B_d \delta_f(k+N_u-1) \\ \quad \vdots \\ x(k+N_p) = A_d^{N_p} x(k) + A_d^{N_p-1} B_d \delta_f(k) \\ \quad + A_d^{N_p-2} B_d \delta_f(k+1) + \cdots + \\ \quad \sum_{i=1}^{N_p-N_u+1} A_d^{i-1} B_d \delta_f(k+N_u+1) \end{cases} \tag{16}$$

In the case $N_u < N_p$, it is assumed that the control input is invariant from N_u step to N_p step, that is $u(k+N_u) = u(k+N_u+1) = \cdots = u(k+N_p-1)$, the output could be predicted as follows:

$$\begin{cases} z(k+1) = C_d A_d x(k) + C_d B_d \delta_f(k) \\ z(k+2) = C_d A_d^2 x(k) + C_d A_d B_d \delta_f(k) \\ \quad + C_d B_d \delta_f(k+1) \\ \quad \vdots \\ z(k+N_u) = C_d A_d^{N_u} x(k) + C_d A_d^{N_u-1} B_d \delta_f(k) \\ \quad + \cdots + C_d B_d \delta_f(k+N_u-1) \\ \quad \vdots \\ z(k+N_p) = C_d A_d^{N_p} x(k) + C_d A_d^{N_p-1} B_d \delta_f(k) \\ \quad + \cdots + \sum_{i=1}^{N_p-N_u+1} C_d A_d^{i-1} B_d \delta_f(k+N_p-1) \end{cases} \tag{17}$$

The N_p step output prediction of system can be expressed as:

$$Z(k) = \Psi X(k) + \Theta U(k) \tag{18}$$

where

$$Z(k) = \begin{bmatrix} z(k+1) \\ z(k+2) \\ \vdots \\ z(k+N_p) \end{bmatrix}; \quad X(k) = \begin{bmatrix} x(k+1) \\ x(k+2) \\ \vdots \\ x(k+N_p) \end{bmatrix};$$

$$U(k) = \begin{bmatrix} \delta_f(k) \\ \delta_f(k+1) \\ \vdots \\ \delta_f(k+N_u-1) \end{bmatrix}; \quad \Psi = \begin{bmatrix} C_d A_d \\ C_d A_d^2 \\ \vdots \\ C_d A_d^{N_p} \end{bmatrix};$$

$$\Theta = \begin{bmatrix} C_d B_d & 0 & \cdots & 0 \\ C_d A_d B_d & C_d B_d & \cdots & 0 \\ \vdots & \vdots & \ddots & \vdots \\ C_d A_d^{N_p-1} B_d & C_d A_d^{N_p-2} B_d & \cdots & \sum_{i=1}^{N_p-N_u+1} C_d A_d^{i-1} B_d \end{bmatrix}$$

The weighted objective functions of lateral displacement, yaw angle and steering angle are defined as follows:

$$J(k) = \sum_{i=1}^{N_p} \|z(k+i) - r(k+i)\|_Q^2 + \sum_{i=1}^{N_u} \|\delta_f(k+i-1)\|_R^2 \quad (19)$$

where $r(k+i) = [y(k+i), \psi(k+i)]^T$, $Q = diag(Q_1, Q_2 \cdots Q_{N_p})$ is the weighting matrix and R is the weighting coefficient.

According to the system constraints, the following optimization problem can be solved in each time step

$$\min_{U(k)} J(k) \quad (20)$$

Subject to :

$$u_{\min}(k+i) \le u(k+i) \le u_{\max}(k+i) \quad i = 0, 1, \cdots, N_u - 1 \quad (21)$$

$$-\Delta u_{\min}(k+i) \le \Delta u(k+i) \le \Delta u_{\max}(k+i) \quad i = 0, 1, \cdots, N_u - 1 \quad (22)$$

$$y_{\min}(k+i) \le y(k+i) \le y_{\max}(k+i) \quad i = 0, 1 \cdots, N_p - 1 \quad (23)$$

where the inequalities (21) limit the control inputs, (22) constrain the changes of the control input, while (23) are constraint on system output variables.

Obviously, this is a constrained optimization problem, which can be transformed into a quadratic programming problem. The specific implementation process will not be detailed here, more details can be seen in reference [13].

2) HUMAN-MACHINE SHARED CONTROL STRATEGY

In order to assist the driver to track the desired path while reducing the risk of rollover, a shared control strategy based on fuzzy control method is designed by considering the road hazard level and the driver steering operation hazard, which is enlightened by [27].

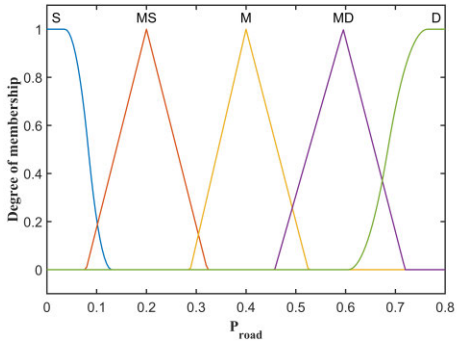

FIGURE 6. Membership function of road hazard.

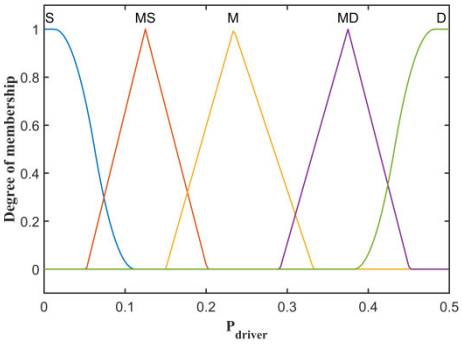

FIGURE 7. Membership function of human steering operation hazard.

The road hazard is employed to recount the vehicle position dangerous as follows:

$$P_{road} = \left| y_p(k) - y_c(k) \right| \quad (24)$$

where $y_p(k)$ is the lateral position of driver's preview point, $y_c(k)$ is the lateral position of road centerline at the driver's preview point.

Considering the driver's current state and behavior, the following parameters are selected to describe the driver steering operation hazard based on the information available from the current scheme, expressed by:

$$P_{driver} = \sigma \left| \delta_{mpc} - \delta_{driver} \right| \quad (25)$$

where $\sigma > 0$ is a regulating factor, δ_{mpc} is the front wheel angle output by MPC controller, δ_{driver} is the front wheel angle output by driver, $\delta_{driver} = \delta_{sw}/i$.

The form of the shared control strategy in this work is enlightened by Anderson *et al.* [28]. The final steering command is the linear weighted sum of the driver's input and the controller's input, denoted as:

$$U_s = \Gamma U_{mpc} + (1 - \Gamma) U_{dri} \quad (26)$$

where U_s, U_{mpc} and U_{dri} refer to the shared steering input, MPC controller's input, and a driver's input, respectively; Γ is the shared coefficient.

Since the shared coefficient is difficult to describe with an accurate formula, and the fuzzy control method is selected and it could be more smooth and effective. Consequently,

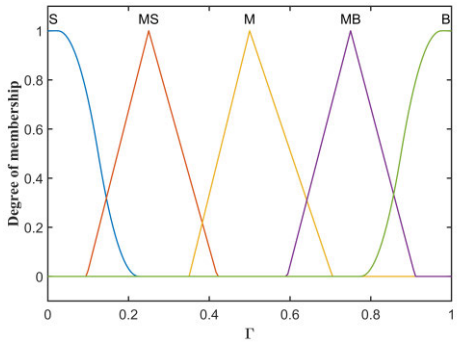

FIGURE 8. Membership function of shared coefficient.

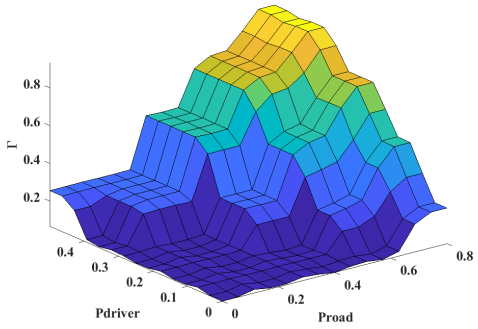

FIGURE 9. Fuzzy regular surfaces.

TABLE 2. Fuzzy control rule base.

P_{road}	P_{driver}				
	S	MS	M	MD	D
S	S	S	S	S	MS
MS	S	S	S	MS	MS
M	S	S	MS	M	M
MD	S	MS	M	MB	MB
D	MS	M	MB	B	B

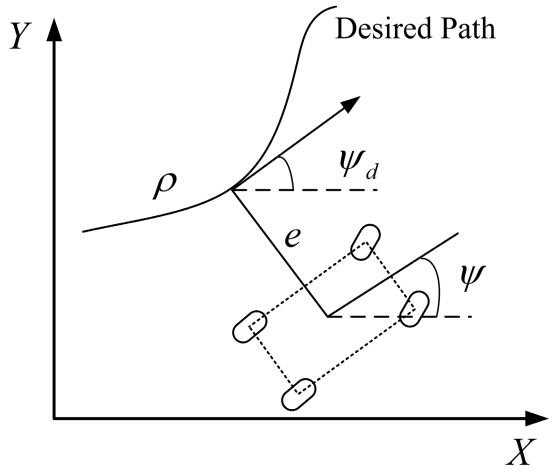

FIGURE 10. Path tracking error dynamics model.

the basic ideas of the fuzzy control strategy based on expert experience are given as follows:

When P_{road} is relatively small, it indicates that the current road risk is low, and the intensity of machine intervention should also be small. When P_{road} is relatively large, it indicates that the deviation of current path tracking is relatively large. If P_{driver} is small, it means that the driver's manipulation behavior is normal, and the shared coefficient Γ should also be relatively small. Otherwise, the shared coefficient Γ increases with the increase of P_{driver}.

1. Fuzzy variables: P_{road} has five associated linguistic values: safe (S), medium safe (MS), medium (M), medium dangerous (MD), dangerous (D). Its membership function shape is shown in Figure 6.

P_{driver} has five associated linguistic values: safe (S), medium safe (MS), medium (M), medium dangerous (MD), dangerous (D). Its membership function shape is shown in Figure 7.

Γ has five associated linguistic values: small (S), medium small (MS), medium (M), medium big (MB), big (B). Its membership function shape is shown in Figure 8.

2. Fuzzy rules: The fuzzy rules are produced based on expert knowledge, and these rules are generated from the simulation experience in our study. All rules can be seen in Table 2 and Figure 9 shows the fuzzy regular surfaces.

3. Defuzzification: The center-of area defuzzification method is utilized in our work.

C. DESIGN OF ACTIVE BRAKING SYSTEM

The active braking controller is designed to reduce the current risk of vehicle rollover under emergency conditions. The active braking system is only activated according to the roll stability evaluation index because the braking system directly affects the longitudinal movement of the vehicle. Since lateral acceleration is the dominant factor of rollover, much research on anti-rollover has pointed out that the lateral acceleration can be reduced by controlling the yaw motion.

1) PATH TRACKING MODEL

The path tracking error dynamics model is shown in Figure 10.

The path tracking error dynamics based on the Serret-Frenet equations are given by:

$$\begin{cases} \dot{\psi}_r = \dot{\psi} - \dot{\psi}_d = r - \rho v_x \\ \dot{e} = v_x \sin \psi_r + v_y \cos \psi_r \end{cases} \tag{27}$$

where ψ_d is the tangential direction of the desired path; e is the vertical distance from vehicle centroid to the desired path; ρ represents the curvature of the desired path; ψ_r is called heading error. Generally, the control objective for the path tracking problem is to design a controller to globally asymptotically stabilize e and ψ_r, and ensure the lateral stability at the same time.

2) DESIRED YAW RATE CALCULATION

Generally, the desired side slip angle is chosen as $\beta_d = 0$. Regarding the calculation of the desired yaw rate, reference [7] used the 2-DOF steady-state yaw rate as the tracking target for anti-rollover control and designed a corresponding integrated controller. Simulation results show that it can effectively improve roll stability. However, calculation of the desired yaw rate based on steering wheel angle information, which is assumed that driver's driving behavior is normal. When the driver is in a state of tension and panic, whose behavior will be abnormal, and the steering wheel angle is extremely unreasonable. Therefore, the desired yaw rate calculated by the 2-DOF steady-state yaw rate will be invalid, and the vehicle will lose path following ability, deviate from the centerline of the road and may hit the road railing.

The traditional path tracking control algorithm based on position deviation often ignores the lateral stability of the vehicle. This section focuses on the design of path tracking controller considering the stability and safety of the vehicle. The path tracking model is established, and the desired yaw rate is generated by using hyperbolic projection based feedback dominance backstepping (HFDB).

Projecting e to a new variable z_1 by hyperbolic sine function $z_1 = \sin\kappa e$, where κ is a positive regulating parameter. The Lyapunov function is defined as:

$$V_{1h} = \frac{1}{2}z_1^2 \tag{28}$$

Differentiating equation (28) yields:

$$\dot{V}_{1h} = \kappa z_1 \cosh\kappa e \left[v_x \frac{\sin\psi_r}{\psi_r}(\psi_r - \alpha_{1h} + \alpha_{1h}) + v_x\beta\cos\psi_r \right] \tag{29}$$

By choosing a virtual variable ψ_r and denoting $\alpha_{1h} = -c_1 z_1$ and $z_{2h} = \psi_r - \alpha_{1h}$, equation (29) can be rewritten as:

$$\begin{aligned}\dot{V}_{1h} = &-\kappa c_1 z_1^2 \cosh\kappa e \cdot v_x \frac{\sin\psi_r}{\psi_r} \\ &+ \kappa z_1 \cosh\kappa e \cdot v_x \frac{\sin\psi_r}{\psi_r} z_{2h} \\ &+ \kappa z_1 \cosh\kappa e \cdot v_x\beta\cos\psi_r\end{aligned} \tag{30}$$

which means that if $z_{2h} = 0$

$$|z_1(\infty)| \le \bar{z}_1(t) = \left| \frac{\beta\psi_r}{c_1 \tan\psi_r} \right| \tag{31}$$

so $z_1 \to 0$, $e \to 0$, as $\beta \to 0$

The second Lyapunov function is defined as:

$$V_{2h} = V_{1h} + \frac{z_{2h}^2}{2c_1^2} \tag{32}$$

Derivation equation (32) and feedback linearization is instead by utilizing feedback dominance to simplify the deduction yields:

$$\begin{aligned}\dot{V}_{2h} = &-\kappa c_1 z_1^2 \cosh\kappa e \cdot v_x \frac{\sin\psi_r}{\psi_r} + \kappa z_1 \cosh\kappa e \cdot v_x\beta\cos\psi_r \\ &- \frac{c_2}{c_1}\kappa \cosh\kappa e \cdot z_{2h}^2 \left[1 - \frac{c_1 v_x}{c_2}\frac{\sin\psi_r}{\psi_r} \right] \\ &+ \frac{1}{c_1^2}\kappa z_{2h}\left[r - \rho v_x + c_1 \cosh\kappa e \cdot v_x\beta\cos\psi_r - \alpha_{2h} \right]\end{aligned} \tag{33}$$

where $\alpha_{2h} = -c_2 z_{2h}\cosh\kappa e$, c_2 is a constant and $c_2 \ge c_1 v_x$, we choose $z_{3h} = r - \rho v_x - \alpha_{2h}$. Thus, if $z_{3h} = 0$, (33) can be simplified as:

$$\begin{aligned}\dot{V}_{2h} = &-\kappa c_1 z_1^2 \cosh\kappa e \cdot v_x \frac{\sin\psi_r}{\psi_r} + \kappa z_1 \cosh\kappa e \cdot v_x\beta\cos\psi_r \\ &- \frac{c_2}{c_1}\kappa \cosh\kappa e \cdot z_{2h}^2 \left[1 - \frac{c_1 v_x}{c_2}\frac{\sin\psi_r}{\psi_r} \right] \\ &+ \frac{1}{c_1}\kappa z_{2h}\cosh\kappa e \cdot v_x\beta\cos\psi_r\end{aligned} \tag{34}$$

which implies:

$$|z_{2h}(\infty)| \le \bar{z}_{2h}(t) = \frac{c_1 v_x\,|\beta\cos\psi_r|}{c_2\left(1 - \frac{c_1 v_x}{c_2}\frac{\sin\psi_r}{\psi_r}\right)} \tag{35}$$

and $z_{2h} \to 0$ as $\beta \to 0$. By making $z_{3h} = 0$, the desired yaw rate can be obtained:

$$r_{\alpha h} = \rho v_x + \alpha_{2h} \tag{36}$$

where $\alpha_{2h} = -c_2 z_{2h}\cosh\kappa e$, $z_{2h} = \psi_r - \alpha_{1h}$ and $\alpha_{1h} = -c_1 z_1$. If $z_1 \to 0$ and $z_{2h} \to 0$, since $z_1 = \sinh\kappa e$, we can conclude that $e \to 0$ and $\psi_r \to 0$, and the path following target is realized if the real yaw rate tracks the desired value $r_{\alpha h}$.

By assuming a small angle for ψ_r and the lateral offset e can be generally assumed very small. Therefore, (36) can be rewritten as:

$$r_{\alpha h} = \rho v_x - c_2 c_1 \kappa (e + \frac{1}{c_1\kappa}\psi_r) \tag{37}$$

The selection rules of parameters in (37) are as follows: c_1 is inversely proportional to v_x, and $c_1 > 0$, $c_2 \ge c_1 v_x$, we choose $c_1 = 2/v_x$, $c_2 = 30c_1$, that is $c_1 = 0.1029$, $c_2 = 3.087$, $\kappa = 0.5$.

More details about controller design can be seen in literature [29].

3) DESIGN OF YAW MOMENT CONTROLLER

A proportional integral differential (PID) controller is adopted to obtain the additional yaw moment according to the error between the expected yaw rate and the actual yaw rate.

$$M_z = K_P\Delta r + K_I\int \Delta r dt + K_D\frac{d\Delta r}{dt} \tag{38}$$

where $\Delta r = r_{\alpha h} - r$, K_P is the proportional gain, K_I is the integral gain, K_D is the differential gain. Here, $K_P = 1400$, $K_I = 500$, $K_D = 10$.

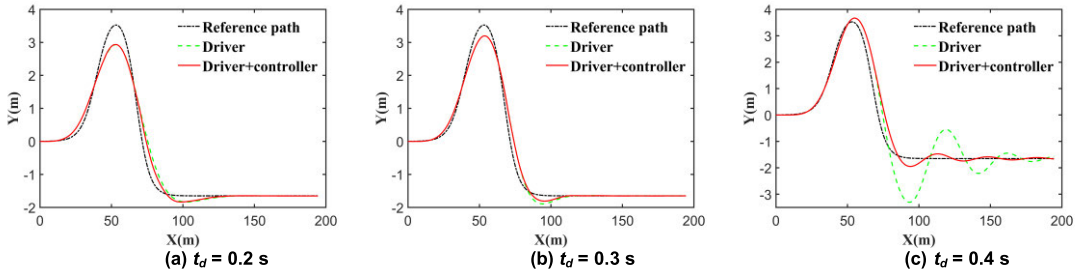

FIGURE 11. Path tracking comparison results.

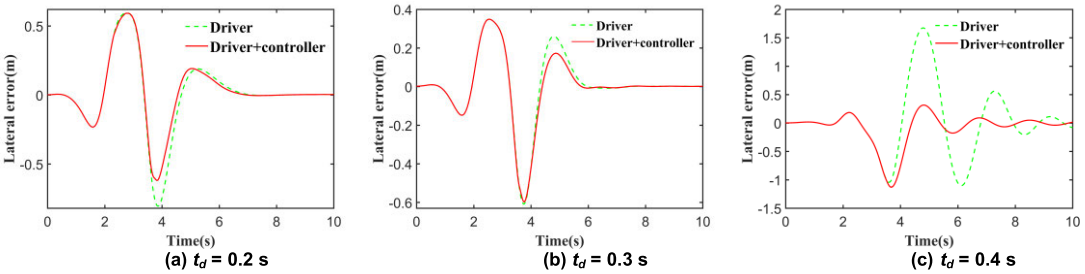

FIGURE 12. Lateral deviation comparison results.

TABLE 3. Braking torque distribution strategy.

States	Braking wheel	Braking torque
$\delta_{sw} > 0, y_{ZMP} > 0$	rear right	$T_{b,rr} = -2RM_z / B$
$\delta_{sw} < 0, y_{ZMP} > 0$	rear right	$T_{b,rr} = -2RM_z / B$
$\delta_{sw} > 0, y_{ZMP} < 0$	rear left	$T_{b,lr} = 2RM_z / B$
$\delta_{sw} < 0, y_{ZMP} < 0$	rear left	$T_{b,lr} = 2RM_z / B$

where R is tire radius, B is rear wheel track.

4) BRAKING TORQUE DISTRIBUTION

The additional yaw moment calculated by PID requires to be allocated to specific wheels, and the yaw stability control of the vehicle is realized by braking only one wheel. Since front wheels are utilized as the driver's steering input, only rear wheels are involved in the control law. Table 3 indicates the allocation principles of wheel selection on the basis of steering wheel angle and the evaluation index of roll.

D. DESIGN OF INTEGRATED CHASSIS CONTROLLER

An integrated chassis controller based on steer-by-wire and active braking is designed for anti-rollover and path tracking control of the autonomous vehicle under critical scenarios. The integrated chassis controller is only turned on at $\int \left|\dot{\delta}\right| dt \geq Th$ and $|y_{ZMP}| \geq 0.7$, when the driver's steering wheel angle changes too much within a period of time and the risk of rollover is high. Due to the limitation of the driver's physiology, psychology and driving skills, it is considered that the driver has no ability to continue driving, so the auxiliary system takes over the vehicle.

The integrated controller is designed by MPC, and the predictive model is select the 2-DOF model in section IIA. The state equation is as follows:

$$\begin{cases} \dot{x} = A_0 x + B_0 u \\ y = C_0 x \end{cases} \tag{39}$$

where $x = [\beta \ r]^T$, $u = [\delta_f \ M_z]^T$, $A_0 = \begin{bmatrix} a_{11} & a_{12} \\ a_{21} & a_{22} \end{bmatrix}$.

$$B_0 = \begin{bmatrix} \frac{2C_f}{mv_x} & 0 \\ \frac{2aC_f}{I_z} & \frac{1}{I_z} \end{bmatrix}, \quad C_0 = \begin{bmatrix} 1 & 0 \\ 0 & 1 \end{bmatrix}.$$

In this section, the desired side slip angle is $\beta_d = 0$, and the desired yaw rate is $r_d = r_{\alpha h}$.

IV. SIMULATION RESULTS AND ANALYSIS

A CarSim and MATLAB/Simulink co-simulation is adopted in our work, and the vehicle parameters used in the simulation process are shown in Table 4. In order to verify the effectiveness of the proposed control strategy, the double lane change maneuver and the fishhook maneuver are selected as simulation conditions.

A. DOUBLE LANE CHANGE MANEUVER

When the vehicle is driving at high speed, the vehicle's roll stability is poor due to the dry road surface and the excessive input of the steering wheel angle. In order to test the effectiveness of the control strategy, the double lane change maneuver is selected as the simulation condition. The speed of the vehicle is set as 70 Km/h and the road adhesion coefficient is set as 0.9. The neural response lag time constant is usually set as $t_d = 0.2 - 0.4$ s. This work chooses $t_d = 0.2$ s to simulate

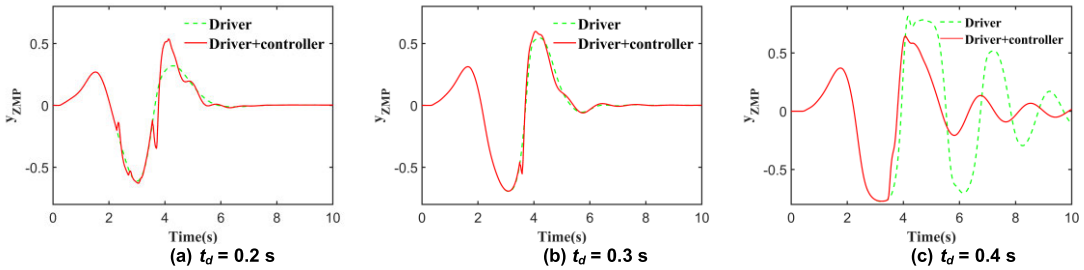

FIGURE 13. Roll stability comparison results.

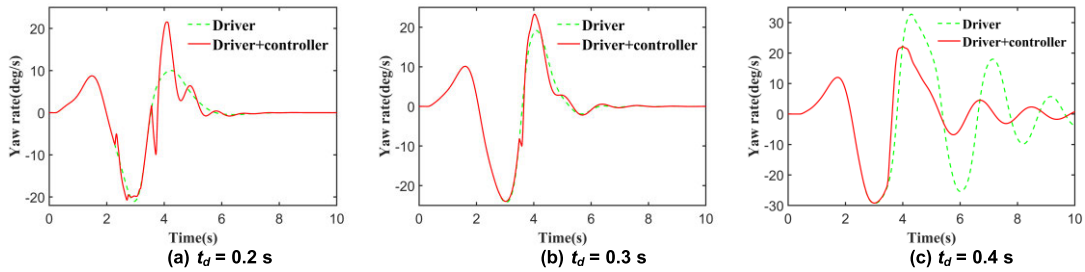

FIGURE 14. Yaw rate comparison results.

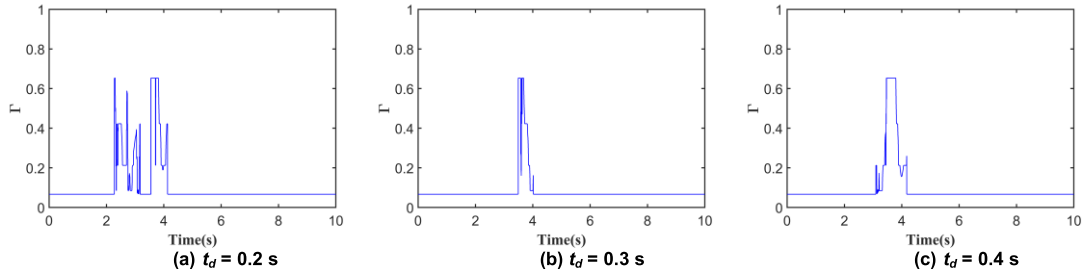

FIGURE 15. Human-machine shared coefficient.

TABLE 4. Main simulation parameters.

Parameter	Value	Unit
m	2532	kg
C_f	145400	N/rad
C_r	145400	N/rad
a	1.33	m
b	1.81	m
I_z	3524.9	kg.m^2
I_x	846.6	kg.m^2
h	0.781	m
D	1.739	m
i	21	
B	1.75	m
L	3.14	m
R	0.368	m

an excited driver; $t_d = 0.3$ s is selected to simulate a normal type of driver; we choose $t_d = 0.4$ s to simulate a physiologically fatigued and distracted driver. Action response lag time constant is usually set as $t_h = 0.05 - 0.2$ s, and because action response lag time has little effect on the roll stability, the action response lag time of three types of drivers is set as $t_h = 0.1$ s. Driver represents the driver's individual control, and Driver + controller represents the collaborative control. The parameters of MPC controller are: $N_p = 25$, $N_u = 10$, $Q = \begin{bmatrix} 10 & 0 \\ 0 & 300 \end{bmatrix}$, $R = 0$.

Figures 11 and 12 show the comparison of path tracking results. It can be concluded from Figures 11(a)-(b) and Figures 12(a)-(b) that the collaborative control can improve the tracking accuracy when the driver's neural response delay time is 0.2 s and 0.3 s. Figure 11(c) and Figure 12(c) show that the collaborative control can significantly improve path tracking accuracy and compensate for the tracking error caused by the driver's untimely response.

Table 5 illustrates the root mean square (RMS) of tracking deviations with the driver's individual control and the collaborative control. It is established that compared with the driver's individual control with $t_d = 0.2$ s, the RMS of path tracking deviation of the collaborative control is 0.236 m, and the tracking accuracy is improved by 11.94%.

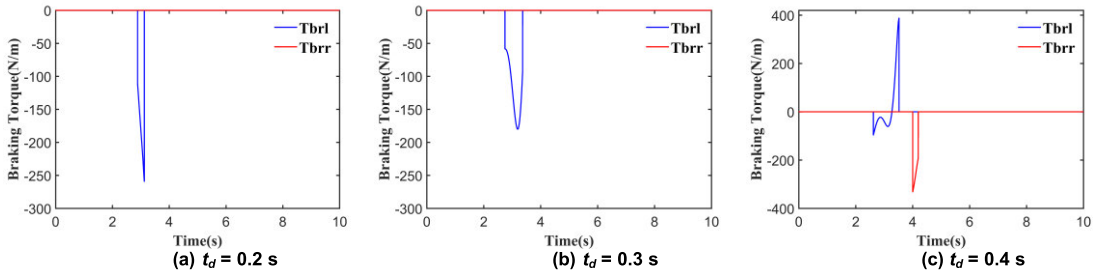

FIGURE 16. Rear wheel braking torque.

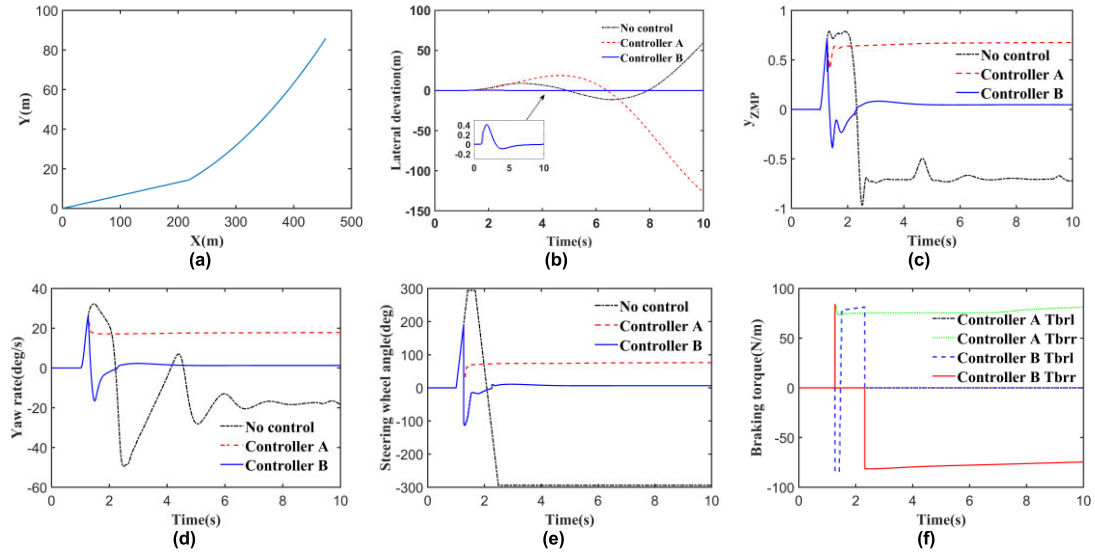

FIGURE 17. Simulation results under fishhook maneuver: (a) road model, (b) path tracking deviation, (c) y_{ZMP}, (d) yaw rate, (e) steering wheel angle, (f) rear wheel braking torque.

It is established that compared with the driver's individual control with $t_d = 0.3$ s, the RMS of path tracking deviation of the collaborative control is 0.173 m, and the tracking accuracy is improved by 3.89%. It is established that compared with the driver's individual control with $t_d = 0.4$ s, the RMS of path tracking deviation of the collaborative control is 0.304 m, and the tracking accuracy is improved by 49.75%.

As it is understood from Figures 13(a)-(b), the roll stability evaluation index y_{ZMP} of collaborative control is basically the same as that of individual control. Although there is an increase at t = 4.2 s, the values are all less than 0.6, which is within a safe range. When $t_d = 0.4$ s, the collaborative control can effectively improve the vehicle's roll stability compared with the individual control. In Figures 14(a)-(b), the yaw rate of collaborative control increases when t = 4.2 s, but decreases rapidly and finally tends to be stable. This is because when roll stability is good, the collaborative control sacrifices a certain degree of roll stability to improve the path tracking accuracy. It can be seen from Figure 14(c) that the collaborative control can effectively improve the yaw stability of the vehicle compared with the driver's individual control with $t_d = 0.4$ s. The human-machine shared coefficient is shown in Figure 15, and the shared controller can adaptively adjust the weight between human and machine to assist different types of drivers. Figure 16 shows that since the human-machine shared steering cannot meet the additional yaw moment requirement, the braking torque is added to guarantee the vehicle's roll stability. Thus, according to the above simulation analysis, it can be concluded that the collaborative controller can adapt to different types of drivers, reduce the operating burden, and obtain good path tracking ability and roll stability.

TABLE 5. Root mean square of path tracking deviation.

Nervous system delay time	Individual control	Collaborative control
$t_d = 0.2$ s	0.268 m	0.236 m
$t_d = 0.3$ s	0.180 m	0.173 m
$t_d = 0.4$ s	0.605 m	0.304 m

B. FISHHOOK MANEUVER

In order to test the roll stability and path tracking performance of the integrated chassis controller in the automatic driving state, the fishhook maneuver is chosen as a test condition. The speed of the vehicle is set as 80 Km/h and the road adhesion

coefficient is set as 0.9, the maximum steering wheel angle is ±294°. The road model is shown in Figure 17(a).

The integrated chassis controller designed in this work is marked as controller B, and the desired yaw rate is generated by HFDB. Another integrated chassis controller designed in literature [7] is marked as controller A, and the desired yaw rate is generated by the 2-DOF model steady-state yaw rate. The parameters of two MPC controllers are: $N_p = 25$, $N_u = 10$, $Q = \begin{bmatrix} 10 & 0 \\ 0 & 100 \end{bmatrix}$, $R = 0$.

It can be seen from Figure 17(b) that controller A and without control cannot track the road center line, and the vehicle deviates from the road. The maximum deviation of the path tracking of controller B is 0.4 m, and it quickly drops to zero, which indicates that controller B has good path tracking ability. In Figure 17(c), the roll stability of the vehicle without control is poor, and the maximum value of y_{ZMP} is close to 1. The value of y_{ZMP} under the control of controller A is stable at 0.6. However, the value of y_{ZMP} under the control of controller B quickly tends to zero, which indicates that controller B has better roll stability. Figure 17(d) illustrates that controller B can significantly improve the lateral stability of the vehicle. Figure 17(e) shows the steering wheel angle. Figure 17(f) illustrates the rear wheel braking torque under the two controllers. According to the analysis of the simulation results, the designed controller can improve roll stability and has good path tracking ability.

V. CONCLUSION

In order to adapt to drivers with different neural response delay, this paper proposes a roll stability and path tracking control strategy considering driver in the loop. The human-machine shared weight allocation strategy and active braking controller are established. The integrated chassis controller is designed to take over the vehicle comprehensively and improve safety. The simulation results show that the proposed control strategy can effectively improve roll stability and has good path tracking ability, and possesses the following characteristics:

1. The human-machine sharing is introduced into the vehicle roll stability control, which improves roll stability and path tracking ability, adapts to different types of drivers, and reduces the driver's operating burden.

2. In the integrated chassis control mode for the autonomous vehicle, the road information and vehicle driving state information are comprehensively considered, and the desired yaw rate is derived by the HFDB method. Hence, the vehicle can track the desired path and ensure lateral stability by tracking the generated yaw rate, which has solved the problem that the traditional anti-rollover control method usually ignores path tracking.

Due to insufficient test conditions, the hardware-in-the-loop test will be carried out to verify the effectiveness of the proposed strategy in the future. Further, the dynamic model considering the coupling of higher degrees of freedom will be established and the decoupling problem of the roll stability control and yaw stability control will be studied. Then, the influence of driver misoperation on the safety system will be further considered.

REFERENCES

[1] (2019). *Nhtsa*. [Online]. Available: https://crashstats.nhtsa.dot.gov/Api/Public/ViewPublication/812826

[2] Y. He, X. Yan, X. Lu, D. Chu, and C. Wu, "Rollover risk assessment and automated control for heavy duty vehicles based on vehicle-to-infrastructure information," *IET Intell. Transp. Syst.*, vol. 13, no. 6, pp. 1001–1010, Jun. 2019.

[3] S. Yim, "Design of a robust controller for rollover prevention with active suspension and differential braking," *J. Mech. Sci. Technol.*, vol. 26, no. 1, pp. 213–222, Jan. 2012.

[4] W. Zhao, Y. Li, and C. Wang, "Robust control of hand wheel torque for active front steering system," *Sci. China Technol. Sci.*, vol. 58, no. 1, pp. 107–116, Jan. 2015.

[5] Y. Zhang, A. Khajepour, and X. Xie, "Rollover prevention for sport utility vehicles using a pulsed active rear-steering strategy," *Proc. Inst. Mech. Eng., D, J. Automobile Eng.*, vol. 230, no. 9, pp. 1239–1253, Aug. 2016.

[6] N. C. Parida, S. Raha, and A. Ramani, "Rollover-preventive force synthesis at active suspensions in a vehicle performing a severe maneuver with wheels lifted off," *IEEE Trans. Intell. Transp. Syst.*, vol. 15, no. 6, pp. 2583–2594, Dec. 2014.

[7] B. Zhu, Q. Piao, J. Zhao, and L. Guo, "Integrated chassis control for vehicle rollover prevention with neural network time-to-rollover warning metrics," *Adv. Mech. Eng.*, vol. 8, no. 2, pp. 1–13, Feb. 2016.

[8] F. Yakub, S. Lee, and Y. Mori, "Comparative study of MPC and LQC with disturbance rejection control for heavy vehicle rollover prevention in an inclement environment," *J. Mech. Sci. Technol.*, vol. 30, no. 8, pp. 3835–3845, Aug. 2016.

[9] P. Gaspar, Z. Szabo, and J. Bokor, "Tracking control by integrated steering and braking systems using an observer-based estimation," in *Proc. Eur. Control Conf. (ECC)*, Kos, Greece, Jul. 2007, pp. 619–624.

[10] H. Imine, L. M. Fridman, and T. Madani, "Steering control for rollover avoidance of heavy vehicles," *IEEE Trans. Veh. Technol.*, vol. 61, no. 8, pp. 3499–3509, Oct. 2012.

[11] X. Qian, C. Wang, and W. Zhao, "Rollover prevention and path following control of integrated steering and braking systems," *Proc. Inst. Mech. Eng., D, J. Automobile Eng.*, vol. 234, no. 6, pp. 1644–1659, Jan. 2020.

[12] H. Li, J. Li, Z. Su, X. Wang, and J. Luo, "Research on active obstacle avoidance control strategy for intelligent vehicle based on active safety collaborative control," *IEEE Access*, vol. 8, pp. 183736–183748, 2020.

[13] Y. Tian, K. Huang, X. Cao, Y. Liu, and X. Ji, "A hierarchical adaptive control framework of path tracking and roll stability for intelligent heavy vehicle with MPC," *Proc. Inst. Mech. Eng., D, J. Automobile Eng.*, vol. 234, no. 13, pp. 2933–2946, Jun. 2020.

[14] Z. Jin, Z. Yan, and W. Zhao, "Influences of driver on vehicle rollover stability and anti-roll control," *Chin. J. Mech. Eng.*, vol. 55, no. 4, pp. 109–117, Feb. 2019.

[15] M. Cao, G. Wu, S. Yan, and X. Qian, "Control strategy of vehicle anti-rollover considering driver's characteristic," *IEEE Access*, vol. 8, pp. 128264–128281, 2020.

[16] B. Soualmi, C. Sentouh, J. C. Popieul, and S. Debernard, "Automation-driver cooperative driving in presence of undetected obstacles," *Control Eng. Pract.*, vol. 24, pp. 106–119, Mar. 2014.

[17] J.-M. Hoc, M. S. Young, and J.-M. Blosseville, "Cooperation between drivers and automation: Implications for safety," *Theor. Issues Ergonom. Sci.*, vol. 10, no. 2, pp. 135–160, Mar. 2009.

[18] C. Sentouh, A. Nguyen, J. J. Rath, J. Floris, and J. Popieul, "Human–machine shared control for vehicle lane keeping systems: A Lyapunov-based approach," *IET Intell. Transp. Syst.*, vol. 13, no. 1, pp. 63–71, Jan. 2019.

[19] W. Chen, L. Zhao, D. Tan, Z. Wei, K. Xu, and Y. Jiang, "Human-machine shared control for lane departure assistance based on hybrid system theory," *Control Eng. Pract.*, vol. 84, pp. 399–407, Mar. 2019.

[20] W. Wang, J. Xi, C. Liu, and X. Li, "Human-centered feed-forward control of a vehicle steering system based on a driver's path-following characteristics," *IEEE Trans. Intell. Transp. Syst.*, vol. 18, no. 6, pp. 1440–1453, Jun. 2017.

[21] W. Wang, X. Na, D. Cao, J. Gong, J. Xi, Y. Xing, and F.-Y. Wang, "Decision-making in driver-automation shared control: A review and perspectives," *IEEE/CAA J. Automatica Sinica*, vol. 7, no. 5, pp. 1289–1307, Sep. 2020.
[22] S. Hong and J. K. Hedrick, "Roll prediction-based optimal control for safe path following," in *Proc. Amer. Control Conf. (ACC)*, Chicago, IL, USA, Jul. 2015, pp. 3261–3266.
[23] R. Rajamani, *Vehicle Dynamics and Control*. Springer, 2011, pp. 27–30.
[24] W. Chen, D. Tan, H. Wang, J. Wang, and G. Xia, "A class of driver directional control model based on trajectory prediction," *Chin. J. Mech. Eng.*, vol. 52, no. 14, pp. 89–97, 2016.
[25] K. Liu, J. Gong, S. Chen, Y. Zhang, and H. Chen, "Dynamic modeling analysis of optimal motion planning and control for high-speed self-driving vehicles," *Chin. J. Mech. Eng.*, vol. 54, no. 14, pp. 141–151, Jul. 2019.
[26] L. Li, Y. Lu, R. Wang, and J. Chen, "A three-dimensional dynamics control framework of vehicle lateral stability and rollover prevention via active braking with MPC," *IEEE Trans. Ind. Electron.*, vol. 64, no. 4, pp. 3389–3401, Apr. 2017.
[27] H. Guo, L. Song, J. Liu, F.-Y. Wang, D. Cao, H. Chen, C. Lv, and P. C.-K. Luk, "Hazard-evaluation-oriented moving horizon parallel steering control for driver-automation collaboration during automated driving," *IEEE/CAA J. Automatica Sinica*, vol. 5, no. 6, pp. 1062–1073, Nov. 2018.
[28] S. J. Anderson, S. C. Peters, T. E. Pilutti, and K. Iagnemma, "An optimal-control-based framework for trajectory planning, threat assessment, and semi-autonomous control of passenger vehicles in hazard avoidance scenarios," *Int. J. Vehicle Auto. Syst.*, vol. 8, nos. 2–4, pp. 190–216, 2010.
[29] C. Hu, R. Wang, F. Yan, and N. Chen, "Output constraint control on path following of four-wheel independently actuated autonomous ground vehicles," *IEEE Trans. Veh. Technol.*, vol. 65, no. 6, pp. 4033–4043, Jun. 2016.

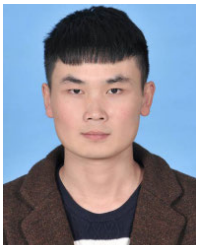

TONGLIANG XU received the B.S. degree from the Anhui University of Science and Technology, Huainan, China, in 2019, where he is currently pursuing the M.S. degree in mechanical engineering. His research interest includes vehicle system dynamics and control.

XUANYAO WANG received the B.S. and M.S. degrees in mechanical engineering from the Anhui University of Science and Technology, Anhui, China, in 2003 and 2006, respectively, and the Ph.D. degree in automotive engineering from the Hefei University of Technology, Anhui, in 2017. He is currently a Professor with the School of Mechanical Engineering, Anhui University of Science and Technology. He has authored more than 20 publications in journals and conference proceedings. His research interests include vehicle system dynamics and control, automotive active safety technology, and advanced driving assistance technology.